NO formation by a catalytically self-sufficient bacterial nitric oxide synthase from *Sorangium cellulosum*

Theodor Agapie[a,b], Sandy Suseno[a], Joshua J. Woodward[a], Stefan Stoll[c], R. David Britt[c], and Michael A. Marletta[a,d,e,f,1]

[a]Department of Chemistry, [d]Department of Molecular and Cell Biology, [e]California Institute for Quantitative Biosciences, and [f]Division of Physical Biosciences, Lawrence Berkeley National Laboratory, and [b]Miller Institute for Basic Science, University of California, Berkeley, CA 94720; and [c]Department of Chemistry, University of California, Davis, One Shields Avenue, Davis, CA 95616

Contributed by Michael A. Marletta, August 5, 2009 (sent for review March 5, 2009)

The role of nitric oxide (NO) in the host response to infection and in cellular signaling is well established. Enzymatic synthesis of NO is catalyzed by the nitric oxide synthases (NOSs), which convert Arg into NO and citrulline using co-substrates O_2 and NADPH. Mammalian NOS contains a flavin reductase domain (FAD and FMN) and a catalytic heme oxygenase domain (P450-type heme and tetrahydrobiopterin). Bacterial NOSs, while much less studied, were previously identified as only containing the heme oxygenase domain of the more complex mammalian NOSs. We report here on the characterization of a NOS from *Sorangium cellulosum* (both full-length, scNOS, and oxygenase domain, scNOSox). scNOS contains a catalytic, oxygenase domain similar to those found in the mammalian NOS and in other bacteria. Unlike the other bacterial NOSs reported to date, however, this protein contains a fused reductase domain. The scNOS reductase domain is unique for the entire NOS family because it utilizes a 2Fe2S cluster for electron transfer. scNOS catalytically produces NO and citrulline in the presence of either tetrahydrobiopterin or tetrahydrofolate. These results establish a bacterial electron transfer pathway used for biological NO synthesis as well as a unique flexibility in using different tetrahydropterin cofactors for this reaction.

heme protein | iron-sulfur cluster | reductase | tetrahydrobiopterin | tetrahydrofolate

Nitric oxide (NO) is recognized as an important signaling molecule as well as a cytotoxin (1–3). A number of diseases are intimately tied to improper function of NO in humans (1–3). Given the importance of NO to human health, a wealth of studies has been performed to address questions regarding NO synthesis and regulation (4–9). Isolation and structural characterization of the proteins responsible for NO synthesis have led to important developments in understanding the molecular processes of NO formation (10–12). Three isoforms of nitric oxide synthase (NOS), iNOS, eNOS, and nNOS, have been characterized in mammals. These enzymes contain an oxygenase domain where the catalysis takes place and a reductase domain that is involved in electron transfer (4, 9). NOS is functional only as a homodimer, and requires the binding of a Ca^{2+}–calmodulin (CaM) complex for electron transfer between the reductase and oxygenase domains. The reductase domain transfers electrons from NADPH (nicotinamide adenine dinucleotide phosphate) via FAD (flavin adenine dinucleotide) and FMN (flavin mononucleotide) to the P450-type heme in the oxygenase domain (13). NOS contains an additional reduced pterin cofactor in the oxygenase domain [H_4B, (6R)-tetrahydro-l-biopterin], which is required for NO formation and is involved in electron transfer processes during catalysis at the heme (14–16).

NOS catalyzes the conversion of Arg into NO and citrulline using O_2 and NADPH involving two catalytic steps. In the first reaction, Arg is oxidized to N^G-hydroxy-arginine (NHA). Nitric oxide is generated in the second half of the cycle, with the conversion of NHA into citrulline. The N-hydroxylation of Arg is proposed to occur via an oxygen-rebound mechanism analogous to the cytochrome P450-type enzymes (6). The second reaction, NHA conversion to citrulline and NO, is unique to NOS. While the mechanism is still under debate, one widely accepted proposal involves a tetrahedral intermediate formed via the nucleophilic attack of a Fe^{III}-hydroperoxo species to NHA (17, 18). In both steps, the tetrahydrobiopterin cofactor is involved in electron transfer (17, 19).

More recently, bacterial NOSs have been reported (20–25). Unlike eukaryotic NOSs, prokaryotic NOSs do not have a reductase domain as a contiguous polypeptide (20, 21) and consequently NO detection has been mostly limited to single turnover experiments (22). In the case of *Bacillus subtilis*, exogenous reductases (a combination of flavodoxin and flavodoxin reductase) were added to NOS, leading to NO formation (determined by the formation of an NOS porphyrin-Fe(III)NO complex and indirectly by nitrite formation) (23). Furthermore, studies with *B. anthracis* and *B. subtilis* which have a gene for a stand-alone oxygenase domain of NOS, indicate that oxygenase domains of bacterial NOSs generate NO by recruitment of intracellular reductases (24, 25).

Herein we report the characterization of a prokaryotic NOS from *Sorangium cellulosum*. This bacterial NOS protein (scNOS) is similar to mammalian NOSs, in that it contains both a reductase and an oxygenase domain in the same polypeptide chain. However, scNOS has distinct differences from the eukaryotic counterpart. Unlike mammalian NOSs, scNOS contains an 2Fe2S ferredoxin subdomain that is involved in electron transfer from NAD(P)H (NADH - nicotinamide adenine dinucleotide—or NADPH) to heme. Furthermore, scNOS can use either tetrahydrobiopterin (H_4B) or tetrahydrofolate (H_4F) for NO formation, a feature unique to scNOS. Purified samples of the full-length enzyme (scNOS) and its oxygenase domain (scNOSox) were shown to generate NO under catalytic and stoichiometric conditions, respectively. The discovery of scNOS provides evidence that nitric oxide synthases evolved from a common ancestor, a NOS oxygenase domain, to include specialized reductase domains both in prokaryotes and eukaryotes.

Results and Discussion

Genetic Similarity Between *S. cellulosum*, Mammalian, and Other Bacterial Nitric Oxide Synthases. A BLAST search using the oxygenase domain of iNOS has predicted homologous proteins in organisms from bacteria to mammals, underscoring the impor-

Author contributions: T.A., J.J.W., R.D.B., and M.A.M. designed research; T.A., S. Suseno, J.J.W., and S. Stoll performed research; S. Stoll contributed new reagents/analytic tools; T.A., S. Stoll, and M.A.M. analyzed data; and T.A., S. Stoll, R.D.B., and M.A.M. wrote the paper.

The authors declare no conflict of interest.

[1]To whom correspondence should be addressed. E-mail: marletta@berkeley.edu.

This article contains supporting information online at www.pnas.org/cgi/content/full/0908443106/DCSupplemental.

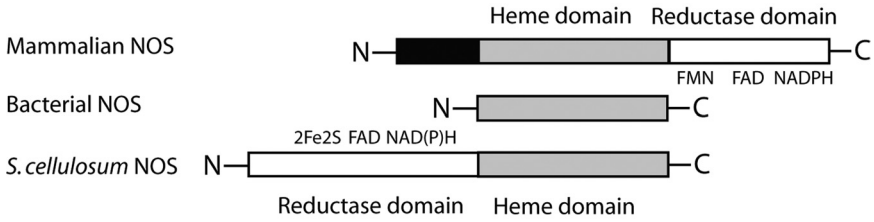

Fig. 1. Comparison of mammalian, bacterial, and *S. cellulosum* nitric oxide synthases. Shown is a schematic of the protein sequences indicating the N- and C-termini and the relative position of the identifiable domains. The heme domains are shown in gray, the reductase domains in white and the N terminus in mammalian NOS without sequence homology in the bacterial NOSs in black. In *S. cellulosum* NOS Fe binding Cys located between amino acid residues 479 and 516.

tance and spread of NOS-like enzymes. Predicted ORFs from *S. cellulosum* (26) contain a putative NOS-like oxygenase domain as part of a larger protein that has another domain which shows significant homology to a reductase domain. Further analysis reveals that the gene for scNOS is predicted to have subdomains corresponding to ferredoxin reductase (FNR), an FAD and NAD(P)H binding protein, and bacterioferritin-associated ferredoxin (Bfd), a 2Fe2S cluster binding protein (Fig. 1). The relative positions of the binding domains for the 2Fe2S cluster, FAD, and NADPH are at the N terminus as shown in Fig. 1 with predicted Fe binding Cys located between amino acid residues 479 and 516. Unlike *S. cellulosum*, all other currently known prokaryotic NOSs contain only the oxygenase domain (25). The oxygenase domain of *S. cellulosum* NOS has significant (over 48%) sequence identity to other bacterial (Fig. S1) as well as to mammalian NO synthases. The NOS from *S. cellulosum* is unique among those from prokaryotes because of the putative reductase domain in the same polypeptide chain. This is similar to mammalian NOS proteins which consist of NADPH, FAD, and FMN binding subdomains. In contrast, scNOS is predicted to contain a 2Fe2S ferredoxin motif, a feature unprecedented for an NOS. Furthermore, the putative reductase domain in scNOS is located at the N terminus while mammalian proteins contain a C-terminal reductase domain.

Cloning, Expression, Purification, and Characterization of scNOS and scNOSox. Constructs for the predicted full-length protein (scNOS) and a truncated construct containing the predicted heme domain (scNOSox) were made. The heme domain construct was selected based on alignment with both the mammalian and bacterial NOS proteins (Fig. S1). The N terminus of the mammalian protein (the first ≈130 amino-acids) is not present in the *S. cellulosum* sequence. This portion of the mammalian protein is involved in dimerization via a zinc tetrathiolate motif and contains some of the pterin cofactor binding residues. Based on homology to other bacterial NOSs, scNOSox was constructed to start at Ala-801 (*S. cellulosum* gene numbering) and to include the C terminus of scNOS (363 amino-acids).

The scNOS and scNOSox constructs were cloned into a pET28b vector encoding an N-terminal His_6-tag with a TEV protease cleavage site and expressed in Tuner (DE3)pLysS cells. scNOS was purified as described in the methods. The final yield of scNOS was 0.4 mg/L. Quantification of cofactors indicates the presence of FAD (0.63 ± 0.02 equiv. relative to the protein concentration determined using a Bradford assay), heme (0.74 ± 0.04 equiv.), and non-heme iron (1.63 ± 0.02 equiv.). The oxygenase domain was purified as described and gave protein (20 mg/L) of purity in excess of 95%. Analytical gel filtration measurements indicate that scNOSox elutes as a monomer and scNOS as a monomer and dimer mixture.

NOS oxygenase domain spectroscopic properties (17, 21) were compared to scNOXox. The Fe(II)-CO, Fe(II)-NO, Fe(III)-NO and imidazole complexes were characterized by UV-vis spectroscopy. The binding of potential substrates and cofactors (Arg, NHA, H_4B, and H_4F) on the Fe(III) spin-state speciation was also investigated. Arg (K_d = 29 ± 4 μM), NHA (K_d = 17 ± 1 μM), and H_4B (K_d = 13 ± 4 μM) were all found to cause a shift in the Soret peak indicative of heme spin-state change. H_4F causes only a small change in absorbance (<0.02) in the Soret band up to concentrations of 600 μM, indicating weak binding or binding without a significant reorganization of the substrate binding pocket. The observed behavior of scNOSox (*SI Text* and Figs. S2 and S3) is generally similar to that of characterized heme domains and bacterial NO synthases suggesting a similar environment.

Single Turnover Studies of scNOSox. The reactivity of scNOSox with oxygen in the presence of substrates and cofactor was investigated. The iNOS oxygenase domain converts NHA to NO in single turnover experiments (17). Following a similar protocol, the scNOSox domain was reduced with a molar equivalent of dithionite and incubated with substrate (Arg or NHA) and cofactor (H_4B, H_4F, or none). Oxygenated buffer was added to solutions above in Reacti-vials and the headspace was tested for NO presence (Fig. S4). NO was detected only in the samples containing cofactors. Samples containing H_4B generate significant amounts of NO, qualitatively similar to the iNOS heme domain under the same conditions. Samples containing H_4F generate smaller, but detectable amounts of NO.

To further investigate the involvement of the tetrahydropterin cofactors in the reaction, stopped flow experiments were performed. Solutions of reduced scNOSox, substrate (Arg or NHA) and cofactor (H_4B, H_4F, or none) were mixed with oxygenated buffer and monitored by electronic absorption spectroscopy (Fig. 2). The conversion of a species with a Soret peak at approximately 430 nm to a species with a Soret peak at approx-

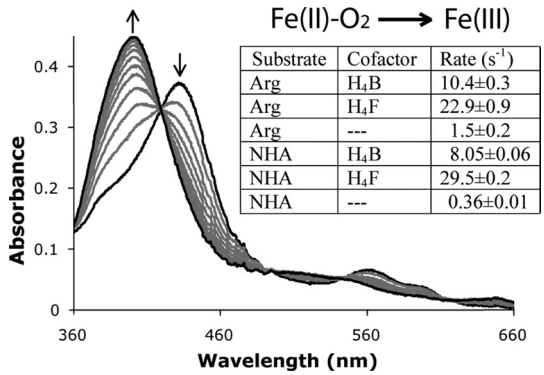

Substrate	Cofactor	Rate (s^{-1})
Arg	H_4B	10.4±0.3
Arg	H_4F	22.9±0.9
Arg	---	1.5±0.2
NHA	H_4B	8.05±0.06
NHA	H_4F	29.5±0.2
NHA	---	0.36±0.01

Fig. 2. Decay of Fe(II)–O_2 and formation of Fe(III) in the presence of H_4B and Arg. Inset: Summary of the rates of Fe(II)–O_2 conversion into Fe(III) in scNOSox in the presence of various substrates and cofactors (see *Materials and Methods* for details).

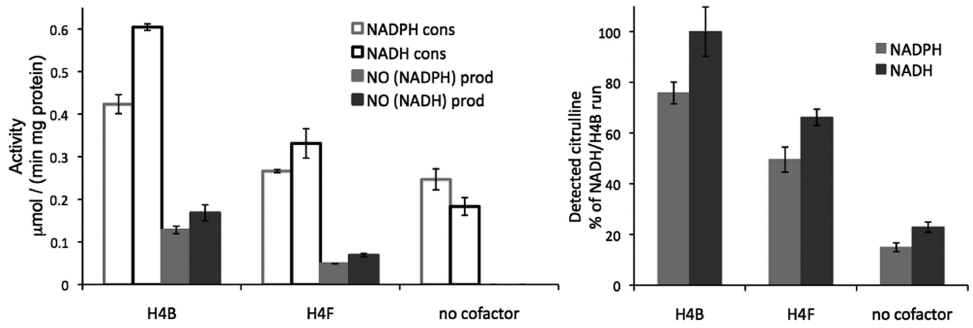

Fig. 3. Catalytic activity of scNOS. (*A*) Initial rates of NADPH and NADH consumption (monitored at A_{340}) and of NO synthesis (monitored at A_{401} using the oxyhemoglobin assay) using reducing equivalents from NADPH and NADH. NO production rate was multiplied by 1.5 to account for the formal utilization of 1.5 NAD(P)H reducing equivalents required for the reaction. (*B*) Citrulline formation (end point measurement) in the oxyhemoglobin assay of scNOS activity. Experiments were performed in triplicate. Error bars represent standard deviations.

imately 400 nm was observed. This was assigned to the transformation of Fe(II)-O_2 to high spin Fe(III). The data fit first order kinetics for this conversion, for all combinations of substrates and cofactors.

Comparison of the rates of conversion from Fe(II)–O_2 to Fe(III) indicates a clear differences between H_4B, H_4F, and no cofactor (Fig. 2, inset). Similar to other NOSs, the presence of a cofactor containing the tetrahydropterin unit increases the rate of conversion of Fe(II)–O_2 by roughly one to two orders of magnitude. In contrast to reports for NOSs from *B. subtilis* and *Deinococcus radiodurans* (for Arg only) (22), H_4F causes a larger increase in rate of Fe(II)–O_2 conversion compared to H_4B with scNOSox. Another distinct feature for scNOSox is the absence of an observable intermediate corresponding to Fe(III)-NO. This could be due to amino acid differences between scNOSox and other NOSs, leading to a faster release of NO from the binding pocket (27).

Overall, the single turnover experiments establish that the heme chemistry in scNOSox is kinetically affected by the presence of either H_4B or H_4F. Furthermore, these results establish that the oxygenase domain is capable of forming NO from NHA in the presence of either tetrahydropterin cofactor, but more efficiently with H_4B. The faster rate of Fe(II)-O_2 to Fe(III) conversion in the presence of H_4F compared to H_4B indicates that the rate-determining electron transfer from tetrahydropterin to heme is faster for H_4F than H_4B; however, subsequent fast steps involved in NO generation must be more efficient for H_4B. Overall, these findings indicate that a tetrahydropterin cofactor capable of electron transfer is necessary for NO formation with scNOSox, behavior similar to related NOS oxygenase domains (16).

Formation of NO with scNOS. Next the role of the reductase domain was investigated using full-length protein, scNOS. Given the prediction of an NAD(P)H binding reductase domain and our studies of scNOSox, the requirements for NO generation were expected to be similar to mammalian NOSs—Arg, O_2, reducing agent (NADPH), and tetrahydropterin cofactor (H_4B or H_4F). Both NADPH and NADH were tested for ability to provide reducing equivalents and both were found to support NO formation. NO formation required either H_4B or H_4F (Fig. S5).

Next the catalytic activity of scNOS was determined (Fig. S6) (28). SOD and catalase were required presumably because of uncoupling. The rate of NO generation was found to be about 2.5-fold higher in the presence of H_4B compared to H_4F. The initial rate of NAD(P)H consumption (Fig. 3*A*) indicates that there is only a small preference for NADH vs. NADPH. The decay of NAD(P)H shows a significantly higher rate of reducing equivalent consumption compared to NO production. NAD(P)H is consumed both in the presence and the absence of cofactor. Compared to NO production, the presence of cofactor leads to a NAD(P)H consumption that is about seven to eight times faster for H_4F and about five to six times faster for H_4B.

To further explore the role of cofactor in catalytic product formation, citrulline was quantified by HPLC (Fig. 3*B*). Mirroring the results of the NO formation assays, more citrulline is generated in the presence of H_4F and H_4B. Compared to apo-protein, H_4F increases the amount of citrulline by about 3-fold while H_4B by about 5-fold. Notably, citrulline forms in the absence of H_4B or H_4F, albeit in smaller amounts. This indicates that the protein is still able to perform substrate activation at the heme; the difference however is reflected in the inability to generate NO in the absence of cofactors.

The present experiments establish the ability of scNOS to catalyze the formation of NO. In the presence of H_4B, the enzyme activity (0.11 μmol NO/min mg protein, at 25 °C) is about 2.5-fold higher than with H_4F (0.046 μmol NO/min mg protein). Quantification of citrulline formed correlates with these findings. Analysis of uncoupling with the two cofactors points to a similar trend. When adjusting the rates of electron flow [from NAD(P)H to NO], H_4B is found to be about 30% coupled while H_4F about 20% coupled (Fig. 3*A*). Part of the significant uncoupling observed in these studies may be due to cofactor loss (heme or 2Fe2S cluster). Nevertheless, these results correlate with the findings of the single turnover experiments in that H_4B leads to more NO production compared to H_4F. Assuming similar binding of cofactor to scNOS (10-fold increase in concentration was found to only slightly affect rates of NO production), this difference suggests that H_4B leads to faster and more efficient NO generation. However, the measured differences between the reactivity of scNOS with the two cofactors are not very large and the ability of this enzyme to use both H_4B and H_4F for catalytic NO formation is most notable.

Investigation of scNOS Reduction with NADPH by EPR and UV-Vis Spectroscopy. EPR samples were prepared anaerobically in the presence of H_4B and Arg. The EPR spectrum in the absence of NADPH (Fig. 4) is indicative of a high spin Fe(III) heme species (14). The absence of a signal from the 2Fe2S cluster indicates that it is in a S = 0, $[Fe_2S_2]^{2+}$ state. Separate samples prepared as above were treated with NADPH; this causes a substantial change in the spectrum–disappearance of the high spin heme-Fe(III) signal. A new signal, however, is detectable with an axial g tensor [$g_\perp$ = 1.922 (5), $g^\parallel$ = 2.019 (5)]. These g values are consistent with a low-spin (S = 1/2) $[Fe_2S_2]^{+}$ cluster (29, 30). The disappearance of the heme high spin Fe(III) signal upon NADPH addition is consistent with reduction of heme to EPR-silent Fe(II), presumably via the flavin and 2Fe2S cluster.

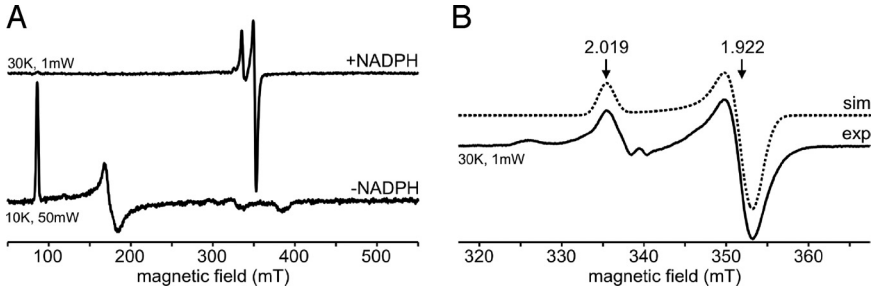

Fig. 4. EPR analysis of scNOS. (*A*) EPR spectra of scNOS in the presence of Arg and H_4B with and without NADPH addition. (*B*) Experimental and simulated spectrum of the sample obtained after NADPH addition. All spectra were acquired at 9.4793 GHz.

The observation of a signal for the 2Fe2S cluster is indicative of the ability of NADPH to cause the reduction of this cofactor, and also stands as additional proof for a unique electron transfer pathway in scNOS.

UV-vis spectroscopy experiments were performed to complement the EPR findings (Fig. S3). Arg and H_4B were added to anaerobic samples containing oxidized protein. UV-vis spectroscopy reveals the presence of high spin Fe(III) heme species. Addition of NADPH, followed by brief purging with CO gas leads to the appearance of a peak at 445 nm (Fig. S3), indicative of the formation of the heme Fe(II)-CO complex. As with the EPR experiments, the generation of the heme Fe(II)–CO species upon NADPH addition is indicative of a functional electron transfer pathway from the biological electron donor (NADPH) to the heme reaction center.

Mechanistic Implications. The results in this paper highlight some significant differences between scNOS and other NOSs. The observed activities for NO production, coupled with the NOA data for the scNOSox protein, clearly show that scNOS is a competent catalyst for the generation of NO from Arg. This makes scNOS unique among bacterial NOSs since all others require additional proteins to mediate electron transfer to heme. A significant difference from mammalian NOS is the presence of a 2Fe2S cluster. Formally the 2Fe2S cluster replaces the FMN cofactor in the mammalian NOSs. The redox potentials of FMN in nNOS are −49 mV (ox/sq, oxidized/semiquinone) and −274 mV (sq/hq, semiquinone/hydroquinone) (31). In nNOS, FAD has redox potentials of −232 mV (ox/sq) and −280 mV (sq/hq) that allow for FMN reduction by FAD. Since in nNOS the heme Fe(II)/Fe(III) potential is −248 mV (with bound Arg and H_4B), FMN (hq) can transfer electrons to ferric heme (32). The redox potential of the 2Fe2S cluster in Bfd is −254 mV, (33) which matches the sq/hq couple of FMN in nNOS and is well suited for electron transfer from FAD to heme. Notably, the redox potentials of the 2Fe2S and flavin cofactors can vary significantly as a function of protein environment. The lack of an EPR signal for FAD sq upon scNOS reduction with NADPH suggests a situation in which both FAD hq and sq can transfer electrons to oxidized 2Fe2S. A proposed electron transfer pathway is presented in Fig. 5. FAD is capable of formally accepting two electrons from NAD(P)H and of performing single electron reductions. These processes lead to the reduction of both the 2Fe2S cluster and the heme. An additional NAD(P)H equivalent can re-reduce FAD leading to a protein state in which all cofactors are reduced. It is noteworthy that by AGF scNOS elutes as an apparent monomer and dimer mixture (the retention times deviate from the calculated molecular weight values; however, the two peaks correspond to a doubling in mass and are most consistent with a monomer and dimer). Hence, more complex mechanisms involving electron transfers between the reductase and oxygenase domains within a dimer are possible and remain to be studied.

The reaction at the heme is proposed to occur in a fashion similar to other NOSs (Fig. 6) (16). The reduced heme binds O_2. An additional electron transfer combined with protonation activates it for the oxygenation of the substrate. Similar to mammalian NOSs, scNOS requires a tetrahydropterin cofactor for catalytic formation of NO (16, 17). This requirement points to a general need for a redox active cofactor in close proximity to the heme, where the catalytic chemistry occurs. Unlike mammalian proteins, however, scNOS is capable of using both H_4B and H_4F as cofactors for NO production. While H_4F was used previously in bacterial NOS studies (21, 22), NO production was directly observed only recently (39). Bioinformatics analysis of *S. cellulosum* suggests that it is capable of H_4B and H_4F biosynthesis, (34) hence, in principle, it could use either of these cofactors for NO formation. It is noteworthy that compared to H_4B, H_4F leads to faster conversion of Fe(II)-O_2 into Fe(III) (scNOSox), but to slower and less efficient NO generation (scNOS and scNOSox). The fundamental reasons behind this behavior may be related to the relative reactivity of the putative $H_3B\bullet$ and $H_3F\bullet$ intermediates. These important mechanistic details remain to be elucidated.

Conclusions

scNOS is an example of a catalytically self-sufficient bacterial NOS. The reductase domain of scNOS is unique in the NOS family by containing a 2Fe-2S ferredoxin cluster. This points to a common ancestor for NOSs—the oxygenase domain. Variants of NOS seem to have evolved to include different types of

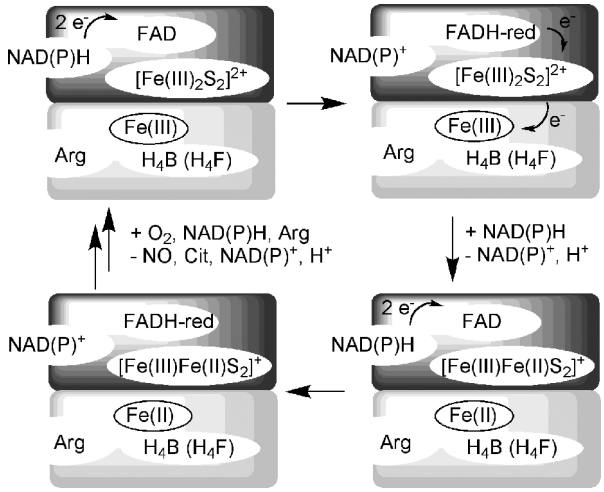

Fig. 5. Proposed electron transfer processes from NAD(P)H to heme via cofactors in the reductase domain.

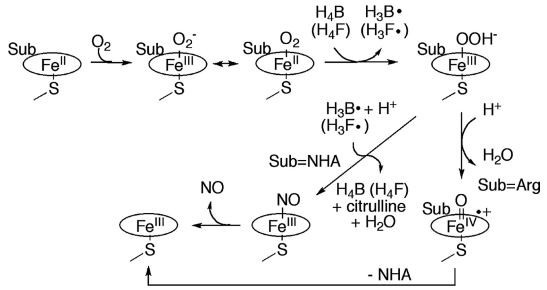

Fig. 6. Proposed mechanism of the chemical reactions at the heme with oxygen, substrates, and cofactors.

reductase domains or no reductase domains. An additional unusual feature of scNOS is the ability to form NO in the presence of either H_4F or H_4B cofactors, providing a unique platform to characterize the efficiency of these two cofactors for generating NO, perhaps leading to insight into the evolution to use H_4B as the preferred cofactor for NO biosynthesis in mammals. The biological significance of this cofactor flexibility for scNOS is not clear, but it may involve a mechanism to control NO production under different conditions. The role that this NOS plays in *S. cellulosum* remains to be defined.

Materials and Methods

Materials. See *SI Text* for details.

Cloning. scNOS cDNA was generated from bacterial artificial chromosomes provided by Prof. Rolf Müller (Institute of Pharmaceutical Biotechnology, University of Saarland, Germany) by PCR using the following primers: 5′-GAGGAGCATATGGCCCTGCC GAGCACCATG-3′ and 5′-GAGGAGAAGCTTC-TACCCCTTCCGCTCCTTCCAC-3′. The scNOSox construct was generated from above bacterial artificial chromosomes by PCR using primers designed to generate *Nde*I and *Hin*dIII cutsites: 5′-GAGGAGCATATGGCGC CCGAGGCG-GTG-3′, and 5′-GAGGAGAAGCTTCTACCCCTTCCGCTCCTTCCAC-3′. Various amounts (5–10%) of DMSO were required for efficient PCR. PCR products were digested with *Nde*I and *Hin*dIII. The genes for scNOS and scNOSox were ligated into the *Nde*I and *Hin*dIII sites of a pET28b vector engineered with a His_6-tag and a TEV cleavage site at the 5′-end to generate plasmids pET28b-scNOS and pET28b-scNOSox. All genetic manipulations were performed using *E. coli* DH5a cells. Purified plasmid DNA and PCR products were sequenced by Elim Biopharmaceuticals Inc. to confirm the absence of mutations.

Protein Expression and Purification. For expression, plasmids containing the desired genes were transformed into Tuner (DE3)pLysS cells. Overnight cultures of Tuner (DE3)pLysS-pET28scNOS were used to inoculate (1/100) expression cultures (1 L of Terrific Broth containing 30 mg/L of kanamycin and chloramphenicol, ultra-yield flasks) at 37 °C. Upon reaching an A_{600} of 0.8, the cultures were cooled to 25 °C and induced by the addition of isopropyl-beta-D-thiogalactopyranoside (IPTG, 0.4 mM final concentration), and harvested by centrifugation 20–22 h after induction.

scNOS. Cell pellets from 9 L of culture were resuspended in lysis buffer (50 mM sodium phosphate, pH 8.0, 10 mM imidazole, 10% glycerol, 10 mg/L benzamidine, 5 mg/L leupeptin, and 1 mg/L each of pepstatin, chymostatin, and antipain, and 1 mM pefabloc) to a total volume of 200 mL and lysed using an Emulsiflex-C5 high-pressure homogenizer. Supernatant was prepared by centrifugation for 1 h at 40,000 × *g* and was loaded by gravity on a 10 mL nickel column (Ni-NTA superflow from QIAGEN). The column was washed with five column volumes (5 × 10 mL) of washing buffer (50 mM sodium phosphate, pH 8.0, 10 mM imidazole). The protein was eluted with 12 mL elution buffer (50 mM sodium phosphate, pH 8.0, 250 mM imidazole). The Ni column was re-equilibrated with washing buffer and the flow through was loaded on the column a second time and washed with five column volumes (5 × 10 mL) of washing buffer, followed by elution with elution buffer. Both elution batches were purified by anion exchange using an HQ8 column and buffer containing 20 mM Tris-HCl, pH 8.0 and 20 mM Tris-HCl, 1 M NaCl, pH 8.0. The scNOS fractions (SDS/PAGE with Coomassie staining) were pooled and concentrated using spin-concentrators with a 50 kDa molecular weight cutoff. Concentrated samples were diluted with TEV protease cleavage buffer (50 mM Tris-HCl, 0.5 mM EDTA, 1 mM DTT, 2 mM imidazole, pH 8), a stock solution of TEV protease was added, followed by incubation at 4 °C for 6–8 h. The buffer was exchanged to washing buffer in three concentration/dilution (higher than 10-fold) cycles. The resulting mixture was loaded on a Ni column and washed with three column volumes (3 × 10 mL) of washing buffer. The flow through was concentrated and buffer exchanged into HEPES (100 mM, pH 7.4), diluted to 20% glycerol concentrated, divided in small aliquots and stored at −80 °C. Protein obtained by this procedure is >95% pure (SDS/PAGE with Coomassie staining) (Fig. S7). Total protein concentration (7.1 mg/mL in first batch and 4.6 mg/mL in second batch for a total average of 1.3 mg/L of culture) was determined using the Bradford assay, against a BSA standard curve, and was corroborated with UV-vis spectroscopy of the heme-imidazole complex. MALDI of a trypsin in-gel digested sample confirmed this protein's identity (>50% coverage). Quantification of FAD, FMN, and heme cofactors was performed by HPLC with calibration against standard curves of commercial samples (17, 35). Non-heme iron content was determined using a spectrophotometric assay using ferene as a chelator (36).

scNOSox. Supernatant was prepared as above and loaded on a nickel column (Ni-NTA superflow from QIAGEN) and washed with five column volumes of washing buffer (50 mM sodium phosphate, pH 8.0, 40 mM imidazole), then eluted with elution buffer as above. The wash fraction was rerun through a nickel column, washed, and eluted. The eluate was purified by anion exchange using an HQ8 column, as for scNOS. Fractions containing iNOSheme were red in color and were pooled on the basis of the A_{280}/A_{429} ratio (ratio of peak <1.3). Protein obtained (40 mg/L) by this procedure is >95% pure (SDS/PAGE with Coomassie staining) (Fig. S7). The His_6-tag was cleaved using the TEV protease. Quantification of heme cofactor was performed by absorption spectroscopy after protein denaturation and by HPLC (37). The Fe(III)-imidazole complex was calculated to have $\varepsilon_{429} = 75 \pm 2\ mM^{-1}cm^{-1}$ by the first method and $\varepsilon_{429} = 87 \pm 1\ mM^{-1}cm^{-1}$ by the second.

Analytical Gel Filtration. AGF was performed on an Agilent 1200 HPLC system using a mobile phase consisting of 200 mM KH_2PO_4, 125 mM NaCl, pH 7.4. A calibration curve was generating using the following standards: thyroglobulin (M_r = 669 kDa, t_r = 8.77 min), yeast alcohol dehydrogenase (150 kDa, 10.58 min), BSA (66 kDa, 10.83 min), ovalbumin (45 kDa, 11.24 min), and cytochrome *c* (12.4 kDa, 12.03 min). The calculated molecular weight for scNOSox is 41.7 and the protein eluted as a single peak, at 11.1 min (42 kDa). The calculated molecular weight for scNOS is 127 and the protein eluted as two peaks, at 10.66 and 10.19 min (84 and 153 kDa, respectively).

Spectroscopic Assays of scNOS Activity. Initial rate of NO formation was measured by the oxidation of oxyhemoglobin to methemoglobin using extinction coefficient ($\Delta\varepsilon_{401}$) of 60,000 $M^{-1}cm^{-1}$ (28). A typical 100-μL assay contained 500 μM substrate (Arg), 6 μM oxyhemoglobin, 0, 10, or 100 μM H_4B (or H_4F), 100 U bovine liver superoxide dismutase, 50 U bovine erythrocyte catalase, 0.5 μM scNOS, and 100 μM NADPH in 100 mM HEPES, pH 7.4. Reactions were initiated by the addition of NADPH. The H_4B and H_4F stock solutions were prepared in DMSO anaerobically. The concentration of the cofactor stocks was determined using ε_{298} of 8.71 $mM^{-1}cm^{-1}$ and 28 $mM^{-1}cm^{-1}$ for H_4B and H_4F, respectively. scNOS stocks were preincubated anaerobically with cofactor (H_4F or H_4B) for 45 min before assays. All reactions were run at 25 °C for 10 min. Cofactor concentrations of 1 μM led to barely detectable levels of NO, 10 μM led to reproducible data, and 100 μM generated only slight differences compared to 10 μM; consequently 10 μM was the concentration used for subsequent assays. Similar reaction conditions were used to assay NAD(P)H consumption (at 340 nm, ε_{340} 6220 $M^{-1}cm^{-1}$). The linear portion of absorbance (A_{401} or A_{340}) vs. time plot (typically 0.2–0.5 min) was used to determine initial rates of NO generation or NAD(P)H consumption, respectively.

Assay of scNOS Activity Using an NO Analyzer. NO formation was detected using an NO analyzer (Sievers model 270). A 40-μL final assay mix contained 500 μM substrate (Arg), 0 or 10 μM H_4B (or H_4F), 100 U bovine liver superoxide dismutase, 50 U bovine erythrocyte catalase, 0.5 μM scNOS, and 100 μM NADPH in 100 mM HEPES, pH 7.4. Reactions were initiated with NAD(P)H in oxygenated buffer. All reactions were run at 25 °C in sealed Reacti-vials (Pierce). NO formation was determined at 2 and 10 min (200 μL of headspace). Citrulline was quantified using HPLC (17).

Single Turnover Experiments with scNOSox. NO formation was detected using the NO analyzer. A 40-μL final assay mix contained 500 μM substrate (NHA), 0 or 200 μM H_4B or 400 μM H_4F, 20–60 μM scNOSox in 100 mM HEPES, pH 7.4. Reactions were initiated with oxygenated buffer. All reactions were run at

BIOCHEMISTRY

25 °C in sealed Reacti-vials. NO formation was measured at 30 s by sampling 200 μL of headspace.

EPR Spectroscopy. EPR spectra were recorded at the CalEPR center at UC Davis, using a Bruker ECS106 spectrometer equipped with a ER4102ST resonator and an Oxford ESR900 cryostat. The field modulation was 1.0 mT at 100 kHz. Spectra were background corrected by subtracting the signal from buffer without protein. Simulations were performed with EasySpin (38). The microwave frequency was measured using a EIP548A frequency counter, and the magnetic field was calibrated with LiF:Li [g = 2.002293 (2)]. The accuracy of the obtained g values is $\pm$ 0.005.

Stopped Flow Experiments. Solutions of scNOSox were reduced with dithionite (one molar equivalent) in an inert atmosphere glove bag by mixing 15 μM scNOSox, 15 μM dithionite, 1 mM substrate, and 0 or 400 μM H_4B or 800 μM H_4F in 100 mM HEPES, pH 7.4. This solution was transferred anaerobically to a stopped-flow syringe (Hi-Tech Scientific) and mixed at 10 °C with an equal volume of buffer saturated with O_2 on ice. Spectroscopic changes were monitored over time and data were fit using global fitting software (Specfit version 3.0.14).

UV-vis Spectroscopy Characterization of Heme Species. Solutions of scNOSox or scNOS were prepared anaerobically because H_4B and H_4F are not air stable. To generate Fe(II) species, dithionite was added under an inert atmosphere (N_2/H_2) in a glove bag. Addition of gaseous ligands was performed through a rubber septum using anaerobic cuvettes. UV-vis spectroscopic characterizations were performed using Cary 300 and Cary 3E UV-visible spectrophotometers. Determinations of spectral binding constants were performed by titrating in substrates or cofactors to a solution of scNOSox and monitoring the change in absorption at 398 and 416 nm. A plot of $\Delta(A_{398}\text{-}A_{416})$ vs. ligand concentration was fitted to the equation $\Delta\Delta A = (\Delta\Delta A_{max} \times [\text{substrate}])/(K_D + [\text{substrate}])$. (KaleidaGraph, Abelbeck Software).

ACKNOWLEDGMENTS. We thank Prof. Rolf Müller (Saarland University, Germany) for providing bacterial artificial chromosomes containing the scNOS gene. This work was supported by the Miller Institute for Basic Science (University of California, Berkeley).

1. Dinerman JL, Lowenstein CJ, Snyder SH (1993) Molecular mechanisms of nitric oxide regulation—Potential relevance to cardiovascular disease. *Circ Res* 73:217–222.
2. Kerwin JF, Lancaster JR, Feldman PL (1995) Nitric oxide—A new paradigm for 2nd messengers. *J Med Chem* 38:4343–4362.
3. Moncada S, Palmer RMJ, Higgs EA (1991) Nitric oxide—Physiology, pathophysiology and pharmacology. *Pharmacol Rev* 43:109–142.
4. Alderton WK, Cooper CE, Knowles RG (2001) Nitric oxide synthases: Structure, function and inhibition. *Biochem J* 357:593–615.
5. Li HY, Poulos TL (2005) Structure-function studies on nitric oxide synthases. *J Inorg Biochem* 99:293–305.
6. Marletta MA, Hurshman AR, Rusche KM (1998) Catalysis by nitric oxide synthase. *Curr Opin Chem Biol* 2(5):656–663.
7. Rousseau DL, Li D, Couture M, Yeh SR (2005) Ligand-protein interactions in nitric oxide synthase. *J Inorg Biochem* 99:306–323.
8. Stuehr DJ, Santolini J, Wang ZQ, Wei CC, Adak S (2004) Update on mechanism and catalytic regulation in the NO synthases. *J Biol Chem* 279:36167–36170.
9. Stuehr DJ, Ghosh S (2000) Enzymology of nitric oxide synthases. *Handbook Exp Pharmacol* 143:33–70.
10. Fischmann TO, et al. (1999) Structural characterization of nitric oxide synthase isoforms reveals striking active-site conservation. *Nat Struct Biol* 6:233–242.
11. Raman CS, et al. (1998) Crystal structure of constitutive endothelial nitric oxide synthase: A paradigm for pterin function involving a novel metal center. *Cell* 95:939–950.
12. Crane BR, et al. (1998) Structure of nitric oxide synthase oxygenase dimer with pterin and substrate. *Science* 279:2121–2126.
13. Sono M, Roach MP, Coulter ED, Dawson JH (1996) Heme-containing oxygenases. *Chem Rev* 96:2841–2888.
14. Hurshman AR, Krebs C, Edmondson DE, Huynh BH, Marletta MA (1999) Formation of a pterin radical in the reaction of the heme domain of inducible nitric oxide synthase with oxygen. *Biochemistry* 38:15689–15696.
15. Wei CC, Crane BR, Stuehr DJ (2003) Tetrahydrobiopterin radical enzymology. *Chem Rev* 103:2365–2383.
16. Hurshman AR, Krebs C, Edmondson DE, Marletta MA (2003) Ability of tetrahydrobiopterin analogues to support catalysis by inducible nitric oxide synthase: Formation of a pterin radical is required for enzyme activity. *Biochemistry* 42:13287–13303.
17. Hurshman AR, Marletta MA (2002) Reactions catalyzed by the heme domain of inducible nitric oxide synthase: Evidence for the involvement of tetrahydrobiopterin in electron transfer. *Biochemistry* 41:3439–3456.
18. Woodward JJ, Chang MM, Martin NI, Marletta MA (2009) The second step of the nitric oxide synthase reaction: Evidence for ferric-peroxo as the active oxidant. *J Am Chem Soc* 131:297–305.
19. Davydov R, et al. (2002) EPR and ENDOR characterization of intermediates in the cryoreduced oxy-nitric oxide synthase heme domain with bound L-arginine or N-G-hydroxyarginine. *Biochemistry* 41:10375–10381.
20. Pant K, Bilwes AM, Adak S, Stuehr DJ, Crane BR (2002) Structure of a nitric oxide synthase heme protein from *Bacillus subtilis*. *Biochemistry* 41:11071–11079.
21. Adak S, et al. (2002) Cloning, expression, and characterization of a nitric oxide synthase protein from *Deinococcus radiodurans*. *Proc Natl Acad Sci USA* 99:107–112.
22. Adak S, Aulak KS, Stuehr DJ (2002) Direct evidence for nitric oxide production by a nitric-oxide synthase-like protein from *Bacillus subtilis*. *J Biol Chem* 277:16167–16171.
23. Wang ZQ, et al. (2007) Bacterial flavodoxins support nitric oxide production by *Bacillus subtilis* nitric-oxide synthase. *J Biol Chem* 282:2196–2202.
24. Shatalin K, et al. (2008) *Bacillus anthracis*-derived nitric oxide is essential for pathogen virulence and survival in macrophages. *Proc Natl Acad Sci USA* 105:1009–1013.
25. Gusarov I, et al. (2008) Bacterial nitric oxide synthases operate without a dedicated redox partner. *J Biol Chem* 283:13140–13147.
26. Schneiker S, et al. (2007) Complete genome sequence of the myxobacterium *Sorangium cellulosum*. *Nat Biotechnol* 25:1281–1289.
27. Wang ZQ, et al. (2004) A conserved Val to Ile switch near the heme pocket of animal and bacterial nitric oxide synthases helps determine their distinct catalytic profiles. *J Biol Chem* 279:19018–19025.
28. Marletta MA, Hevel JM (1994) Nitric oxide synthase assays. *Methods Enzymol* 233:250–258.
29. Blumberg WE, Peisach J (1974) Interpretation of electron paramagnetic resonance spectra of binuclear iron sulfur proteins. *Arch Biochem Biophys* 162:502–512.
30. Bertrand P, Guigliarelli B, Gayda JP, Beardwood P, Gibson JF (1985) A ligand-field model to describe a new class of 2fe-2s clusters in proteins and their synthetic analogs. *Biochim Biophys Acta* 831:261–266.
31. Noble MA, et al. (1999) Potentiometric analysis of the flavin cofactors of neuronal nitric oxide synthase. *Biochemistry* 38:16413–16418.
32. Presta A, Weber-Main AM, Stankovich MT, Stuehr DJ (1998) Comparative effects of substrates and pterin cofactor on the heme midpoint potential in inducible and neuronal nitric oxide synthases. *J Am Chem Soc* 120:9460–9465.
33. Quail MA, et al. (1996) Spectroscopic and voltammetric characterization of the bacterioferritin-associated ferredoxin of *Escherichia coli*. *Biochem Biophys Res Commun* 229:635–642.
34. Alm EJ, et al. (2005) The MicrobesOnline web site for comparative genomics. *Genome Res* 15:1015–1022.
35. Light DR, Walsh C, Marletta MA (1980) Analytical and preparative high-performance liquid chromatography separation of flavin and flavin analog coenzymes. *Anal Biochem* 109:87–93.
36. Kennedy MC, et al. (1984) Evidence for the formation of a linear (3fe-4s] cluster in partially unfolded aconitase. *J Biol Chem* 259:4463–4471.
37. Woodward JJ, Martin NI, Marletta MA (2007) An *Escherichia coli* expression-based method for heme substitution. *Nat Methods* 4:43–45.
38. Stoll S, Schweiger A (2006) EasySpin, a comprehensive software package for spectral simulation and analysis in EPR. *J Magn Reson* 178:42–55.
39. Reece SY, Woodward JJ, Marletta MA (2009) Synthesis of nitric oxide by the NOS-like protein from *Deinococcus radiodurans*: A direct role for tetrahydrofolate. *Biochemistry* 48:5483–5491.